HEWLETT hp PACKARD

COMPONENTS

APPLICATION NOTE 962

Silicon Double-Drift IMPATT Diodes for High-Power CW Microwave Applications

CONTENTS

I. INTRODUCTION

II. DEVICE PHYSICS AND CONSTRUCTION
- a. Advantages of the Double-Drift Structure
- b. Chip Fabrication

III. MICROWAVE CIRCUITS
- a. Equivalent Circuits
- b. Coaxial and Waveguide Cavities

IV. MICROWAVE PERFORMANCE AND CHARACTERISTICS
- a. Dependence on Operating Frequency
- b. Large Signal Effects
- c. Dependence on Bias Current

V. INJECTION LOCKING AND NOISE
- a. Injection Locking and External Q
- b. FM Noise

Other relevant HP Application Notes:

AN 935, Microwave Power Generation and Amplification using IMPATT Diodes – a general introduction to IMPATT diode physics, construction and operation.

AN 959-1, Factors Affecting Silicon IMPATT Diode Reliability and Safe Operation – a short note on how to keep an IMPATT diode alive.

AN 961, Silicon Double-Drift IMPATT Diodes for Pulsed Applications – outlines the operating conditions and circuitry required for the proper application of double-drift IMPATT diodes designed for pulsed applications.

INTRODUCTION

Early research into the device physics of avalanche transit-time structures lead first to the development of the P+NN+ single-drift silicon IMPATT diode[1]. This device is now one of the few commercially available sources of CW micro-wave and millimeter-wave power. Considerable improvement in the CW and pulsed performance specifications of silicon IMPATT diodes has recently been achieved by Hewlett-Packard's development of practical devices utilizing the double-drift P+PNN+ structure[2]. The purpose of this application note is to outline the advantages of the double-drift structure in general and provide useful information about circuits and operating characteristics for the CW devices in HP's family of silicon double-drift IMPATT diodes.

DEVICE PHYSICS AND CONSTRUCTION

Advantages of the Double-Drift Structure

The dynamic negative resistance of most IMPATT diode structures results principally from the avalanche and transit-time delay of charge carriers that are injected by impact ionization near a reverse biased PN junction. The same basic mechanism is thus responsible for the microwave generating and amplifying capabilities of both the familiar P+NN+ single-drift device and the superior P+PNN+ double-drift device.

A comparison of the physical structure and the internal doping profile of single and double-drift silicon IMPATT diodes designed specifically for CW operation at 12 GHz is given in Figure 1. The electric field profiles are shown for the reverse bias voltage that results in avalanche breakdown. The avalanche zone, where electron and hole generation occurs, is restricted to a narrow region near the peak electric field because of the highly nonlinear dependence of the electron and hole ionization rates on electric field. The holes generated in the avalanche zone of the single-drift device are immediately collected by the P+ contact while the electrons enter the drift region where they experience a transit-time delay. Both the electrons and holes in the double-drift device experience a transit-time delay in their separate drift regions.

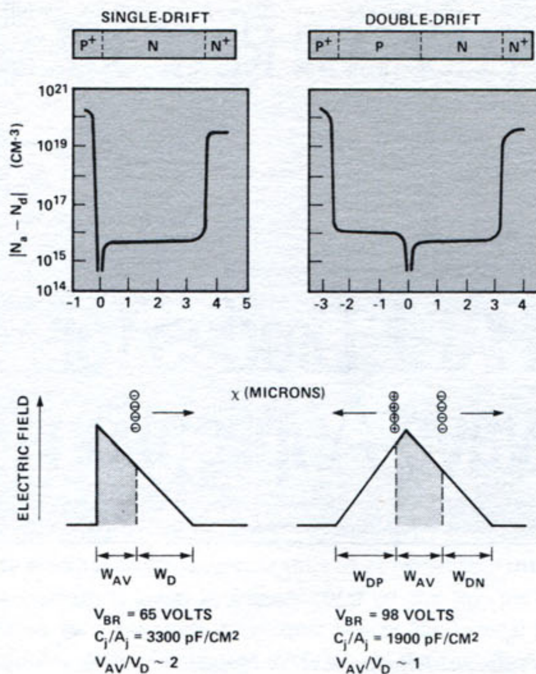

Figure 1. Comparison of the structure of single-drift and double-drift IMPATT diodes. The impurity concentration profiles and the electric field profiles at breakdown are shown.

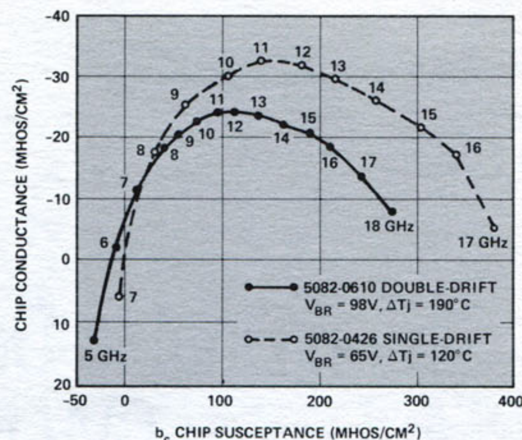

Figure 2. Typical normalized small-signal admittance of single-drift and double-drift IMPATT diode chips biased at a current density of 600A/cm². Junction areas equal 2×10^{-4} cm².

An optimized double-drift IMPATT diode design will not have either equal N and P region widths or equal impurity concentrations because of differences in the characteristics of electrons and holes in silicon. The center of the avalanche zone is shifted into the N region because the ionization rates of electrons are greater than these of holes. The effective drift velocity of holes is less than that of electrons and as a result equal transit-times will occur only if the P drift region is narrower than the N drift region. Double-drift IMPATT diode designs that properly consider these two effects will be electronically symmetrical with equal electron and hole transit times.

One significant advantage of the double-drift structure results from the total depletion layer width at breakdown being approximately 60% wider than a single-drift structure designed for the same frequency. The capacitance per unit area, C_j/A_j, of the double-drift device is thus less than that of the companion single drift device. As a result the chip susceptance per unit area is minimized by using the double-drift structure. Double-drift diodes with large active areas and high power generating capabilities can thus be easily resonated at the desired frequency.

A direct comparison of the small-signal microwave characteristics of typical single and double-drift IMPATT diodes designed for operation at 12 GHz is given by the admittance plane plot shown in Figure 2. This data was obtained for both diodes biased to the same current density and then normalized to the junction area. The frequency dependence of the admittance of both devices is representative of IMPATT diodes in general. The chip conductance is negative over a rather wide frequency range centered at approximately 12 GHz. The susceptance is capacitive over most of the frequency range of negative conductance, but becomes inductive near the low frequency end of the operating band where the conductance becomes positive. The frequency where the susceptance changes sign is generally referred to as the avalanche resonance frequency since it is determined mainly by the inductive nature of the avalanche process and by the capacitance of the device's depletion region. For a particular device the avalanche resonance frequency is determined by the bias current density and the junction temperature. In theory the avalanche resonance frequency increases as the square root of the current density.

The small-signal admittance gives some indication of the wide useful operating frequency range of double-drift silicon IMPATT diodes. Figure 2 shows that the chip conductance of the double-drift device is negative over an approximately 1.6 octave frequency range from 5.9 to 19 GHz. The corresponding range of negative conductance for the single-drift device extends only from 7.2 to 17.5 GHz. The magnitude of the small-signal growth factor, defined as the ratio of chip negative conductance to chip susceptance, can be taken as an indicator of relative power generating capability. The data shown in Figure 2 indicates that the growth factor for the double-drift structure is superior to that of the single drift structure over a broad frequency range.

Simple theoretical considerations[3] have shown that the maximum efficiency at which an IMPATT diode can convert dc input power to microwave power is related in first order to the ratio of the voltage in the avalanche zone, V_{AV}, to the voltage in the drift zone, V_D by

$$\eta \ \alpha \ \frac{1}{1 + V_{AV}/V_D} \tag{1}$$

The ratio of V_{AV}/V_D for the single and double-drift IMPATT diodes shown in Figure 1 is approximately 2 and 1 respectively. Equation (1) thus indicates that the efficiency of double-drift devices should be 1.5 times the typically 7.5% efficiency of single-drift silicon IMPATT diodes. That

Table I. Typical CW Double-Drift IMPATT Diodes

Parameter	Symbol	Optimum Frequency f_{oo} – GHz		
		12 GHz (5082-0610)	12 GHz (5082-0611)	15.5 GHz
Output Power	P_o	1.75 W	2.8 W	2.8 W
Efficiency	η	11%	10.5%	10.5%
Bias Current	I_{OP}	130mA	220mA	270mA
Oscillation Threshold Current	I_{th}	~50mA	~80mA	~100mA
Bias Voltage	V_{OP}	122V	122V	98V
Breakdown Voltage	V_{BR}	99V	99V	78V
Junction Capacitance at Breakdown	$C_{j(V_{BR})}$	0.4 pF	0.8 pF	1.0 pF
Temperature Coefficient of V_{BR}	V'_{BR}	.116V/°C	.116V/°C	.091V/°C
Total Thermal Impedance*	θ_T	14.0°C/W	8.0°C/W	8.0°C/W
Junction Temperature Rise	ΔTj	<200°C	<200°C	<200°C
Space Charge Resistance	R_{SC}	30Ω	15Ω	10Ω
Small-Signal Avalanche Resonance Frequency at I_{OP}	f_{av}	6.6 GHz	6.2 GHz	7.8 GHz
Number of Mesas	–	1	2	2
Package Outline	–	46	46	46

Some useful experimental scaling relationships:

1. $f_{oo} = 2800\,(V_{BR})^{-1.19}$ GHz
2. $V'_{BR} = .117\,(V_{BR}/100)^{1.03}$ V/°C
3. $R_{sc} = .045\,(V_{BR})^{1.21}/C_j$ ohms (C_j units – pF)
4. $f_{av} \propto (I_{OP})^{.37}$

*Measured with the diode mounted in an OFHC copper heat sink using a tellurium copper collet.

the efficiency of double-drift IMPATT diodes is about 11% supports the idea that the efficiency improvement is a result of the reduction of the ratio of V_{AV} to V_D.

The improved efficiencies and high output power capabilities of practical double-drift IMPATT diodes are revealed by Table I which lists the rf specifications and operating parameters of devices designed for center frequencies of 12 and 15.5 GHz.

Chip Fabrication

The fabrication technology for producing IMPATT diode chips is of considerable importance since it strongly affects yield, reproducibility and reliability. The silver-plated heat sink technology developed for single-drift IMPATT diodes[4] is also well suited for double-drift devices.

Perhaps the most important point in the construction of a double-drift device is the epitaxial growth of the active N and P layers on the highly doped N+ substrate. Precise control of the impurity concentrations and widths of the N and P layers are required in order to insure proper device performance.

The contact metalization of the silicon mesa has a major influence on the long term reliability of an IMPATT diode. A metalization scheme was developed for the double-drift IMPATT diode family which allows extremely reliable operation at junction temperatures of 250°C. A cross section of a completed chip is shown in Figure 3.

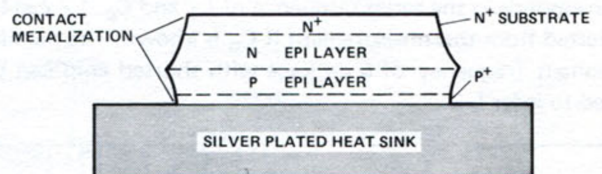

Figure 3. Plated heat-sink double-drift IMPATT diode chip.

MICROWAVE CIRCUITS

Individual chips with one or more mesas can be bonded into standard microwave ceramic packages or directly into microwave integrated circuits. A cross section of a ceramic stud package that is particularly well suited for X- and Ku-band operation of high-power double-drift IMPATT diodes is shown in Figure 4. The low ceramic height of this package results in a low parasitic inductance that mitigates the difficulty of resonating high junction capacitance devices. When soldered into an OFHC copper heat sink the stud package has a lower thermal impedance and superior mechanical ruggedness than alternative threaded designs.

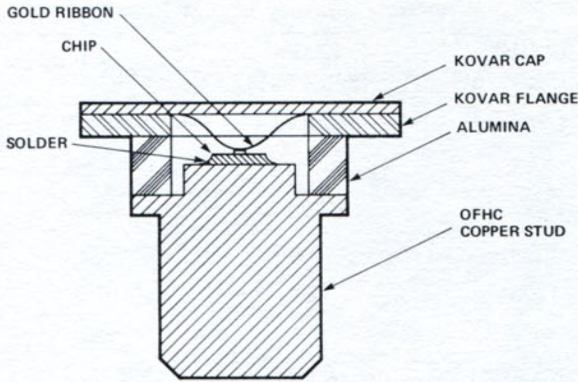

Figure 4. Cross section of IMPATT diode chip in style 46 package.

Equivalent Circuit

The circuit shown in Figure 5 can be a useful lumped element equivalent for both the chip and the package over a broad frequency range. The package is modeled at the plane of the cap by two capacitors and two inductors with frequency independent values. The package capacitance, C_p, is mainly determined by the ceramic dielectric. The mesh capacitance, C_m, corresponds to the small shunt capacitance between the gold contacting mesh ribbon and package stud. The microwave values of C_p and C_m can be taken as equal to the values obtained by 1 MHz capacitance bridge measurements. The inductance L_2 resides in the contacting mesh while L_1 may be thought of as an external inductance arising from the magnetic energy stored in the cylindrical region around the package. Because of its origin, L_1 is highly dependent on the mounting arrangement. The values of L_1 and L_2 can be determined using an automatic network analyzer in a manner similar to that used by Monroe[5]. The series resonant frequency of a package with no contacting mesh corresponds to the series resonance of L_1 and C_p. L_1 can be inferred from this measurement if C_p is known. The parallel resonant frequency of a package with shorted chip can be used to infer L_2.

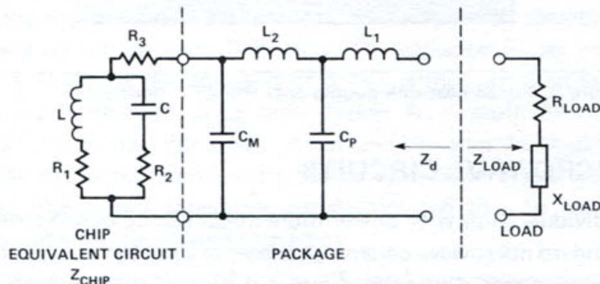

PACKAGE 46 (NO RECESS)		
PARAMETER	DESCRIPTION	TYPICAL VALUE
L_1	EXTERNAL INDUCTANCE	0.26 nH (MOUNT DEPENDENT)
L_2	MESH INDUCTANCE	0.15 nH
C_P	PACKAGE CAPACITANCE	0.55 pF (CAN VARY FROM 0.4 TO 0.6 pF)
C_M	MESH CAPACITANCE	0.05 pF

Figure 5. Equivalent circuit of packaged IMPATT diode chip.

The appropriateness of the values determined for the four elements can be checked by measuring the impedance over a broad frequency range of an IMPATT diode with a known value of junction capacitance at the breakdown voltage. The chip can be taken as a pure capacitance under this condition. Small changes may then be made in L_1 and L_2 in order to bring about good agreement between experiment and the equivalent circuit. If the values for the elements in the equivalent circuit are carefully determined then the style 46 package can be accurately modeled to frequencies higher than 18 GHz. Typical values of L_1, L_2, C_p and C_m are given in Figure 5 for a nonrecessed style 46 package.

Obtaining a simple equivalent circuit for the active chip that is valid under all operating conditions is a difficult task. The chip impedance, $R_{chip} + jX_{chip}$, is highly dependent on bias current, frequency, rf voltage level and junction temperature. It is possible, however, to determine a simple lumped element equivalent circuit that is valid for a restricted range of operating conditions. The five element chip equivalent circuit shown in Figure 5 was developed by Gupta[6] to fit the experimental frequency dependence of IMPATT diode chip admittance such as is illustrated in Figure 2 for fixed bias current conditions. The elements in the equivalent circuit do not have physical significance except for C which can be taken as equal to the junction capacitance at breakdown and L which is related to the avalanche inductance.

Accurate data can be obtained of the small-signal admittance of an IMPATT diode chip by making automatic network analyzer measurements of a packaged diode and subtracting the independently determined package equivalent circuit. It is then possible to select values for the five elements in the chip equivalent circuit that will accurately model the small-signal chip admittance over a wide frequency range from the avalanche resonant frequency to the upper frequency for negative chip conductance. Equivalent circuit element values that give excellent agreement between the model and typical experimental data are given in Table II for both single and double mesa 12 GHz cw diodes biased to 120mA and 200mA respectively. A comparison is given in Figure 6 of the total equivalent circuit impedance, including the package, and the experimental diode impedance.

The small-signal equivalent circuit is helpful in the computer aided design of IMPATT diode oscillators and amplifiers if the circuits can be accurately modeled. For example, the small-signal gain-bandwidth properties of an IMPATT diode in a coaxial amplifier circuit could be easily studied using this diode equivalent circuit. In a stable amplifier the circuit load resistance presented to the diode at any reso-

Table II. IMPATT Small-Signal Equivalent Circuit Elements

Device	R1 (Ω)	R2 (Ω)	R3 (Ω)	L (nH)	C (pF)
5082-0610 I_{OP} = 120mA	17.5	11	−15.5	1.8	0.4
5082-0610 I_{OP} = 200mA	9	5	−7.5	1.0	0.8

nant frequency must be greater than the magnitude of the diode negative resistance. For free-running oscillations the diode impedance, Z_d, will be exactly the negative of the load impedance, Z_{load}.

The usefulness of the equivalent circuit can be extended to practical large-signal conditions where the chip impedance is dependent on rf chip voltage amplitude by allowing both L and R_1 to be dependent on the voltage amplitude[6]. In this case data would be required of both chip conductance and susceptance versus rf voltage for frequencies in the range of interest. Data will be presented in a later section on the effect of rf voltage on chip conductance. The effect of rf voltage on chip susceptance is less pronounced.

Coaxial and Waveguide Cavities

The cross-section of a simple coaxial cavity that is well suited for low-impedance cw double-drift IMPATT diodes operated at frequencies up to 12.4 GHz is shown in Figure 7. Bias is applied through a low shunt capacitance bucket-choke bias "T" similar to that described in AN 935[4]. The transformation from the 50 ohm transmission line to the diode impedance is made by a fixed low impedance section of transmission line immediately adjacent to the diode.

The resonant frequency of a particular diode in this cavity is determined by the length of the transformer section, the depth of the package top and stud recess, the thickness of the spacer and the reactance of the active chip. Data is presented in Figure 8(a) on the effect of changing the diode recess depth, R, and spacer thickness, S, on the resonant frequency of typical single and double-mesa double-drift IMPATT diodes. The principal effect of increasing R or decreasing S is a reduction in the inductance L_1 of the package equivalent circuit. The experimentally inferred dependence of L_1 on R and S is shown in Figure 8(b).

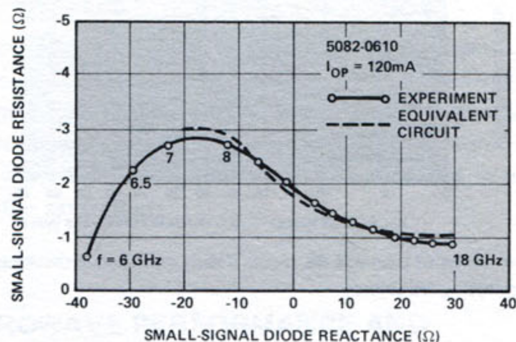

a) Single mesa 5082-0610 diode.

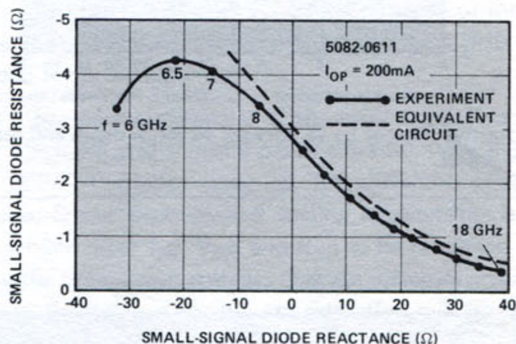

b) Double mesa 5082-0611 diode.

Figure 6. Typical small-signal diode impedance at the plane of the package cap for 12 GHz double-drift IMPATT diodes mounted in 50 ohm, 7 mm coaxial transmission line with zero package recess. Equivalent circuits use chip element values listed in Table II.

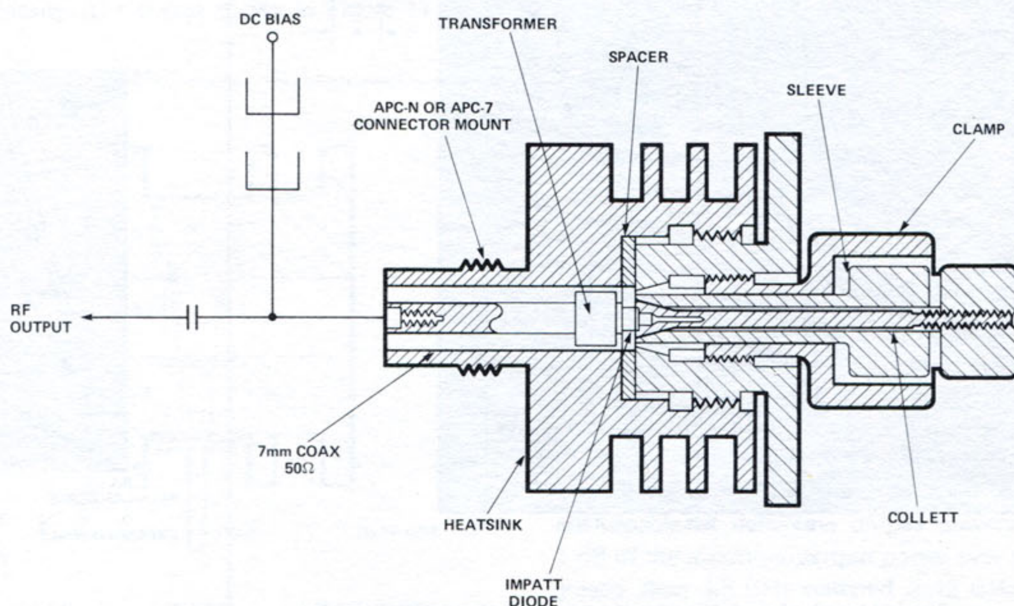

Figure 7. Cross section of fixed single transformer coaxial cavity.

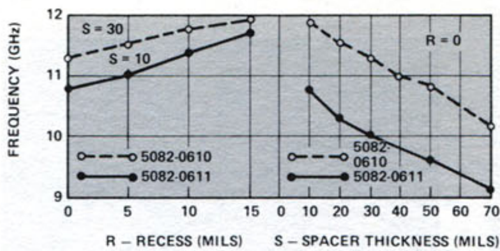

a) Influence of package 46 recess depth and spacer thickness on operating frequency.

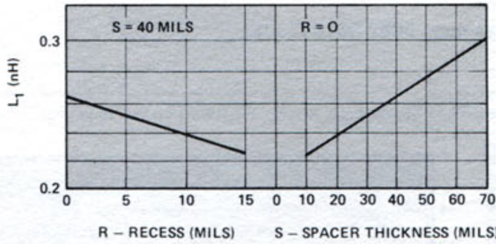

b) Effective value of L_1 vs. package 46 recess depth and spacer thickness.

Figure 8

The curves shown in Figure 9 are useful in the determination of the proper transformer length and characteristic impedance Z_O for operation of a diode at a particular frequency or output power. The usefulness of the curves will be illustrated by two examples using the 5082-0610 diode. Figure 6(a) shows that for R = 0, the diode small signal reactance at 11 GHz is approximately 4 ohms. Figure 15(a) shows that the optimum load resistance is 0.8 ohms for maximum output power at a bias current of 120mA. Since the effect of signal level on diode reactance is relatively small, the desired diode load impedance is thus $Z_{load} = 0.8 - j4$ ohms. The curves in Figure 9(a) reveal that a transformer with a characteristic impedance of 5 ohms and a length of 0.14λ will provide approximately the desired load impedance. For higher resonant frequencies the increasing inductive reactance of the diode would require even shorter transformers. At 13 GHz the proper load impedance for a 5082-0610 has been found to be about .65 - j11 ohms for R = 0. Figure 9(a) reveals that this load impedance could not be achieved even for the shortest practical transformer length. The use of transformers with electrical lengths less than λ/8 is not recommended in any case because R_{load} is too critically dependent on ℓ for ℓ less than λ/8. For high frequency operation it is recommended that λ/8 transformers with the

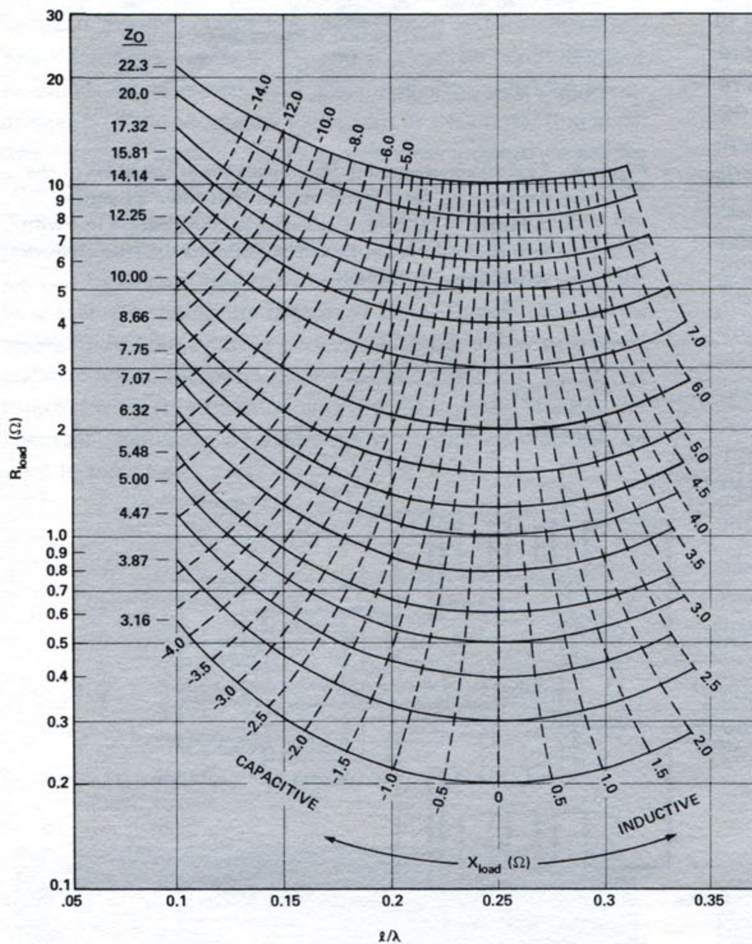

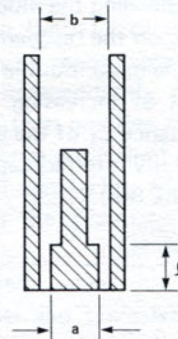

a) Load reistance vs. electrical length of single-step transformer in 50 ohm transmission line. Dashed lines correspond to equal load reactance for transformers with different values of Z_O.

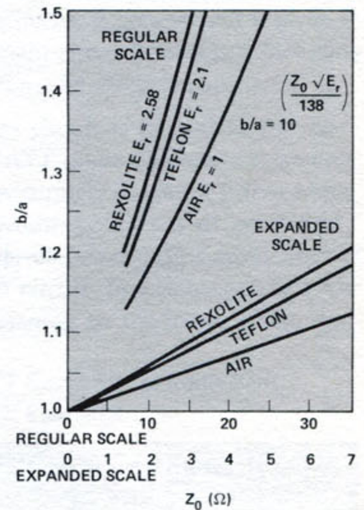

b) b/a versus Z_O.

Figure 9.

proper Z_O be used to provide the desired R_{load} and that R and S be changed to reduce the diode reactance to the value that results in the desired resonant frequency. The curves in Figure 9(b) are useful in finding the value of b/a that will result in the desired transformer characteristic impedance Z_O.

The small differences in the optimum values of R_{load} for individual diodes of the same type may make it desirable to have continuous control over R_{load}. This tuning capability is best achieved by using a coaxial cavity with a fixed transformer that provides an R_{load} greater than the optimum value, positioning a tuning screw at the proper distance from the diode and adjusting its depth to maximize the output power. The best position for the screw can be found empirically by selecting one of three possible positions made available near the diode and spaced approximately $\lambda/8$ apart. Great care must be taken to insure that the diode is not presented with a value of R_{load} that is less than that which maximizes output power since such an overloaded condition can lead directly to diode failure.

In many cases a waveguide cavity may be desired because of requirements for high Q, stability or minimum resistive power loss at high frequencies. Unfortunately it is much more difficult in waveguide to avoid multi-resonant situations or overloading at fundamental or harmonic frequencies. The cross section of a waveguide cavity that has been found to be particularly well suited for using low impedance cw double-drift IMPATT diodes as oscillators and amplifiers is shown in Figure 10. In this cavity the load impedance presented to the diode is determined by the diode package recess, the depth that the coaxial section penetrates into the waveguide, the diameter of the coaxial section and the post that contacts the diode, and the position of the shorting plane. Additional tuning flexibility can be obtained by adding a slide-screw tuner between the cavity and the load. Unfortunately the complexity of this waveguide cavity requires that dimensions for proper tuning be mainly determined empirically. The curves shown in Figure 11 can, however, serve as a rough but useful guide for selecting ℓ and the ratio a/b.

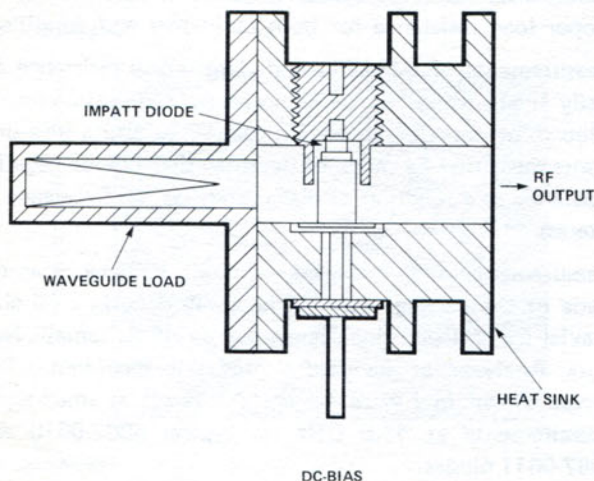

Figure 10. Cross section of double-post waveguide cavity.

The waveguide load that is positioned at the shorting plane of the cavity shown in Figure 10 is for the next higher frequency band. This feature has been found to be highly effective in damping the poorly controlled harmonic signals that can result in tuning induced failures and premature amplifier saturation.

MICROWAVE PERFORMANCE AND CHARACTERISTICS

Information will be presented in this section on the microwave performance and general operating characteristics that must be considered in order to achieve an effective application of cw double-drift IMPATT diodes. Some of the information may also be valuable in the use of double-drift diodes designed for pulsed applications.

Table I presents a summary of the most important microwave, electrical and thermal parameters for typical double-drift IMPATT diodes designed for different center frequencies. Some experimental scaling relationships are also given which allow f_{oo}, V_{BR} and R_{SC} to be predicted for devices with breakdown voltages that are different from those listed in the table. Detailed consideration will be given to the characteristics of the single and double mesa devices that were designed for operation centered at a frequency of approximately 12 GHz.

Dependence on Operating Frequency

The wide frequency range for small-signal negative resistance exhibited by double-drift devices has already been discussed in reference to the admittance-plane plot shown in Figure 2 for a single-mesa 12 GHz chip. The frequency dependence of the small-signal impedance of packaged chips has been presented in Figure 6 for typical 5082-0610 and 5082-0611 diodes whose important parameters are listed in Table I. Oscillation is possible over almost the entire frequency range where the small-signal resistance is negative. Large-signal effects and the small magnitude of the negative resistance at the extremes of the active range, however, restrict useful power generation and amplification to a narrower frequency range.

The power generating capabilities as a function of operating frequency for typical 5082-0610 and 5082-0611 diodes are illustrated in Figure 12. These results were obtained using the coaxial cavity illustrated in Figure 7. The load resistance was carefully adjusted to result in maximum output power at each resonant frequency. The bias current was adjusted in each case to produce a junction temperature rise of 200°C. The curves reveal that these double-drift IMPATT diodes are capable of delivering output powers that are within 1 dB of the maximum output power over a frequency range greater than 4.5 GHz centered at 12 GHz. The percentage bandwidth over which silicon double-drift IMPATT diodes can generate useful output power is superior to all other IMPATT diode structures made from either Si or GaAs.

Figure 11. Load resistance vs. electrical length of coaxial section loaded by a 200 ohm transmission line. Dashed lines correspond to equal load reactance for transformers with different values of Z_O.

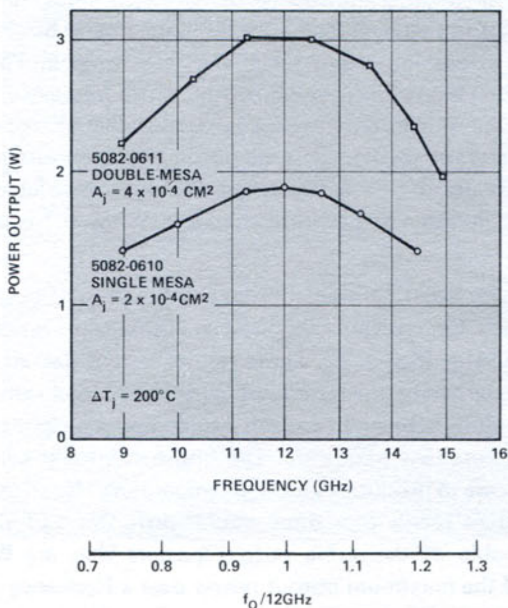

Figure 12. Maximum obtainable output power vs. operating frequency for typical 12 GHz double-drift IMPATT diodes operated with a junction temperature rise of 200° C.

Large-Signal Effects; Amplifier Implications

The saturation of IMPATT oscillator output power or amplifier power gain is the result of the decrease in diode negative resistance caused by increasing rf voltage amplitude. Detailed information about the large-signal resistance of double-drift IMPATT diodes is useful in determining the proper load resistance for both oscillators and amplifiers.

Measurements of IMPATT diode large-signal resistance are easily made using the oscillation-threshold technique developed by Van Iperan and Tjassens[7]. Accurate measurements must first be made of the small-signal diode negative resistance as a function of bias current at the frequency of interest.

Measurements of the small-signal diode impedance at the plane of the package cap can be easily done in a 50 ohm coaxial transmission line using either an HP Automatic Network Analyzer or standard slotted line techniques. The curves shown in Figure 13 are the result of small-signal measurements at 11.5 GHz on typical 5082-0610 and 5082-0611 diodes.

The curves of small-signal diode negative resistance versus current can be used to infer the load resistance which an

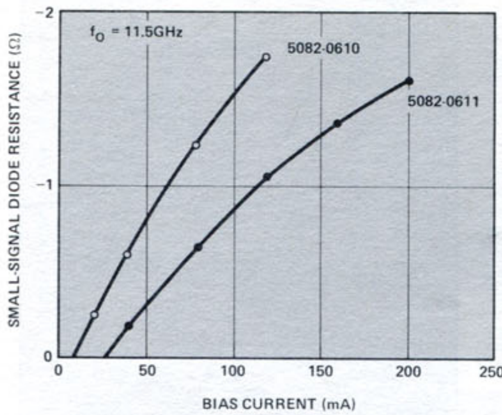

Figure 13. Small-signal diode resistance at 11.5 GHz vs. bias current for typical 5082-0610 and 5082-0611 diodes. Diodes were mounted in 50 ohm, 7 mm coaxial transmission line with zero package recess.

oscillator circuit presents to a diode. The magnitude of an oscillating diode's large-signal negative resistance is always exactly equal to the circuit load resistance at the frequency of oscillation. The diode reactance must first be resonated at a single frequency near the frequency where the small-signal measurements were made. If the bias current of a diode is increased slowly then the diode will begin to oscillate at the bias current where the magnitude of the small-signal negative resistance becomes equal to the circuit load resistance. Typical curves of output power versus bias current for different fixed load resistances are shown in Figure 14 for 5082-0610 and 5082-0611 diodes. In each case

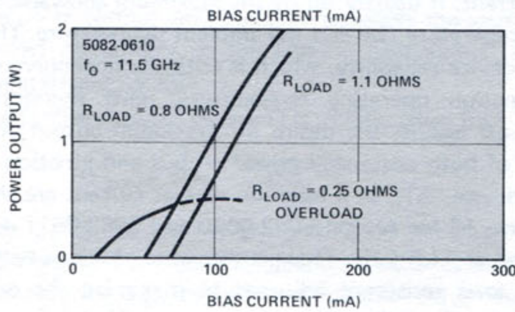

a) 5082-0610

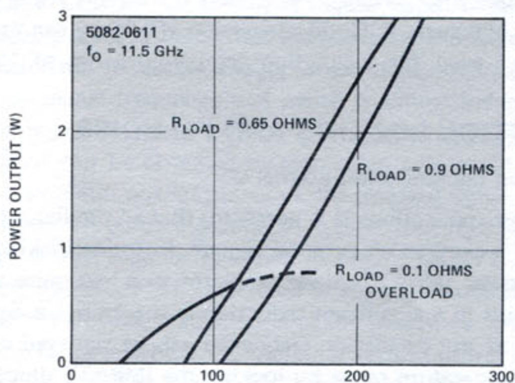

b) 5082-0611

Figure 14. Output power of typical 5082-0610 and 5082-0611 diodes vs. bias current for different values of circuit load resistance.

the value of R_{load} was obtained by noting the threshold bias current and then referring to the data presented in Figure 13. A useful rule-of-thumb is that the threshold current that corresponds to optimum tuning will be approximately 0.37 times the desired operating current.

By using the oscillation threshold technique it is easy to obtain information about the influence of load resistance on obtainable output power from any diode biased to a particular current. Typical curves of output power versus load resistance are illustrated in Figure 15 for 5082-0610 and 5082-0611 diodes. In each case the output power increases as the load resistance is reduced below the value that is equal to the magnitude of the small-signal negative resistance. The maximum power is reached when the rf diode voltage no longer increases with decreasing load resistance. The optimum load resistance is usually between one-third and one-half the magnitude of the small signal negative resistance.

The actual large-signal chip negative conductance can be obtained using the oscillation threshold technique and the package equivalent circuit that has been discussed previously. The amplitude of the rf voltage across the chip is given by

$$\sqrt{2 P_o / |g_c|}$$

where

$$|g_c|$$

is the magnitude of the negative chip conductance. Curves of both output power and chip conductance as a function of rf chip voltage are given in Figure 16 for a 5082-0611 diode. The curves graphically illustrate that power saturation results due to the rapid decrease in chip negative resistance that occurs when the rf voltage amplitude exceeds approximately 35% of the DC bias voltage.

The dependence of large-signal diode resistances on power output that can be inferred from the curves in Figure 15 are useful for predicting amplifier gain compression characteristics[8]. If the load resistance, R_L, is greater than the magnitude of the small-signal diode negative resistance, $|R_{do}|$, then the power gain at the resonant frequency is given by

$$G = \left[\frac{R_L + |R_d|}{R_L - |R_d|}\right]^2 \qquad (2)$$

where R_d is the large-signal diode negative resistance. If K is the ratio of R_d to R_{do} then it can be shown that

$$G = \left[\frac{\sqrt{G_o} + 1 + K(\sqrt{G_o} - 1)}{\sqrt{G_o} + 1 - K(\sqrt{G_o} - 1)}\right]^2 \qquad (3)$$

where G_o is the small-signal amplifier gain.

The value of K is usually about 0.4 for silicon double-drift IMPATT diodes at their full saturated output power. If G_o is 20 dB then equation (3) predicts a saturated power gain of 5.9 dB. The use of equation (3) to predict amplifier performance is only valid if the diode is resonant at a single frequency and if higher harmonic voltages do not result in premature gain saturation.

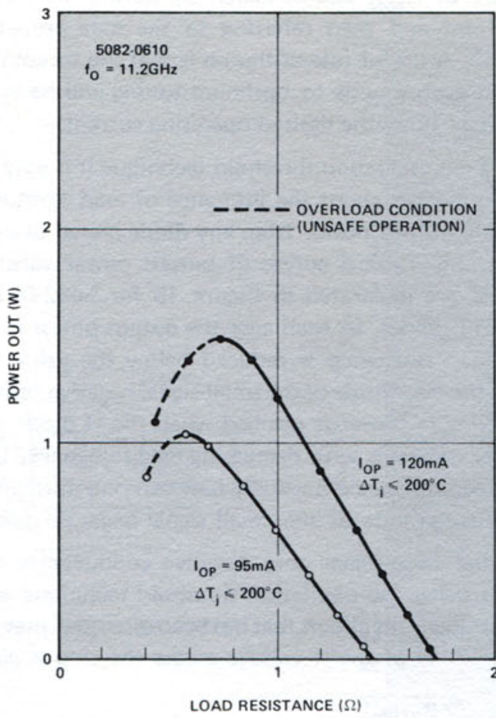

a) 5082-0610

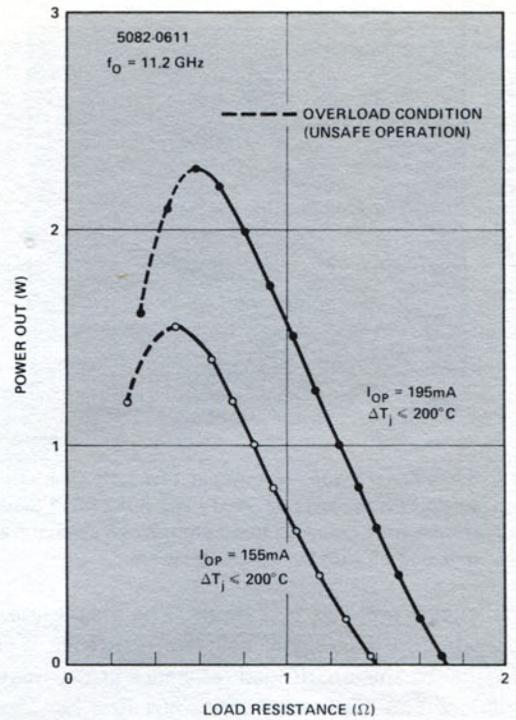

b) 5082-0611

Figure 15. Influence of circuit load resistance on output power of typical 5082-0610 and 5082-0611 diodes biased at constant operating current.

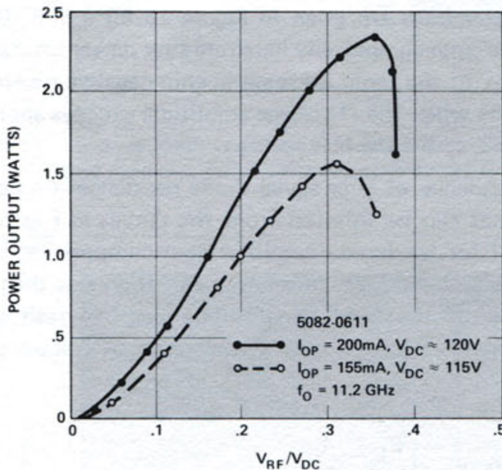

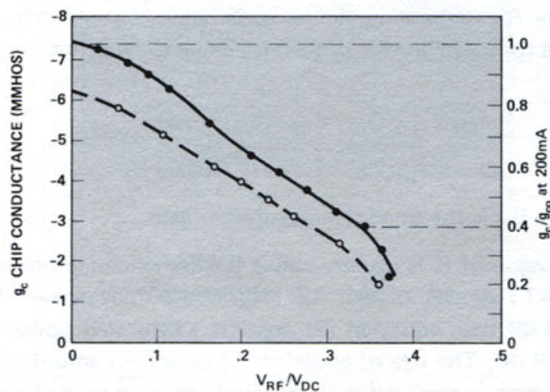

Figure 16. Output power and chip conductance vs. normalized rf voltage for typical 5082-0611 diode.

Dependence on Bias Current

The obtainable output power of any well designed cw IMPATT diode oscillator is always an increasing function of bias current. The upper limit on dissipated power, and thus bias current, is usually set by the maximum allowable junction temperature rise and the ambient temperature. The intrinsic device reliability, which is critically dependent upon the junction operating temperature, must therefore be traded off against the desire for maximum output power. Curves of both optimized power output and junction temperature rise, ΔT_j, as a function of bias current are shown in Figure 17 for typical 5082-0610 and 5082-0611 diodes operated at 11.5 GHz. These curves were obtained with the circuit load resistance adjusted to maximize the output power at each setting of the bias current. Under these load conditions the conversion efficiency is a steeply rising function of bias current. Good conversion efficiency can thus be achieved even for a junction temperature rise of 150°C.

INJECTION LOCKING AND FM NOISE

Injection Locking and External Q

In many applications it is necessary that an oscillator be injection locked to an external signal[9]. Injection locking of a high power IMPATT diode oscillator to a low noise signal can result in a significant reduction in the fm noise. Stabilization of the oscillation frequency can be achieved over a wide temperature range by locking the IMPATT diode to a stable low-power signal. Double-drift IMPATT diodes operated in simple coaxial cavities can be easily phase locked to an external signal injected via a broadband coaxial circulator.

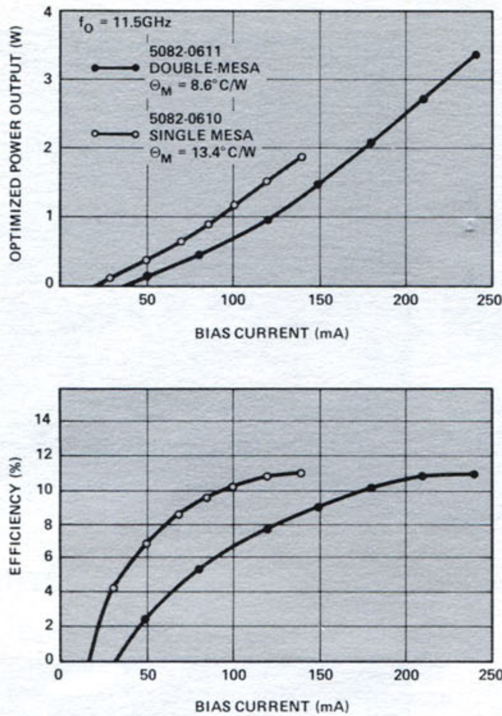

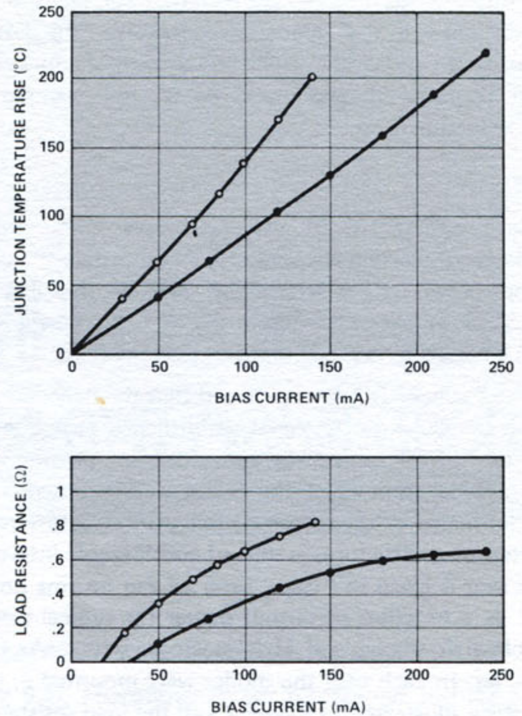

Figure 17. Influence of operating current on optimized output power, efficiency, junction temperature rise and required circuit load resistance for operation of typical 5082-0610 and 5082-0611 diodes at 11.5 GHz. Load resistance was adjusted at each current to result in maximum output power.

The typical locking behavior of a high power 5082-0611 diode tuned for a free-running oscillation frequency of 11.5 GHz is shown in Figure 18(a). The nonlinear diode characteristics that result in dependence of diode susceptance on rf voltage amplitude are probably the cause of the observed asymmetry in the locking gain about the free-running frequency f_O.

The effective external circuit Q is usually given by

$$Q'_{ext} = \frac{f_O}{\Delta f} \sqrt{1/G_L} \qquad (4)$$

Where G_L is the locking gain and Δf is the magnitude of the difference between the injection frequency and f_O. Unfortunately the Q'_{ext} derived from equation (4) is dependent on the frequency of the injected signal for a locking characteristic such as that shown in Figure 18(a). A technique has been proposed which uses the oscillator's locking ellipse characteristic to define a Q'_{ext} which does not involve the injected signal frequency and which is almost independent of the oscillator power output[10]. The locking ellipse of an oscillator can be obtained by displaying a detected replica of the oscillator output power vs. the injected signal's swept frequency on an oscilloscope. A typical locking ellipse obtained in this manner is shown in Figure 18(b). A characteristic frequency $\Delta f'$ is defined as the difference between the ellipse's center frequency and the frequency within the locking range at which the oscillator output power is equal to the free-running oscillator output power, P_O. The effective external circuit Q is then given by

$$Q_{ext}' = \frac{f_O}{\Delta f'} \sqrt{\frac{P_{inj}}{P_O}} \qquad (5)$$

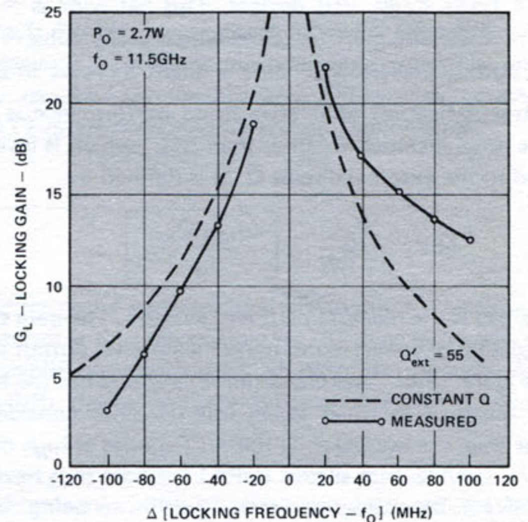

a) Locking gain of 5082-0611 vs. the difference between the injection frequency and the free-running frequency. Q_{ext}' was measured by locking ellipse technique.

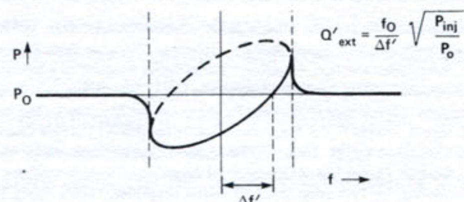

b) Locking ellipse defined by detected oscillator output power vs. swept injection frequency with injection power kept constant.

Figure 18

where P_{inj} is the constant power of the swept injection signal. The definition of Q_{ext}' given by equation (5) has the distinct advantage that it is almost independent of the device parameters and can be identified solely with the external circuit. A Q_{ext}' of 55 was measured for the example illustrated in Figure 18(a).

FM Noise

The noise characteristics of any microwave source are a limiting factor in certain applications. For example the useable output power of a P+NN+ single-drift silicon IMPATT diode must often be limited due to the rapid increase in excess noise which occurs at high output powers.

For IMPATT diodes it has been found that the dependence of fm and am noise on rf signal amplitude is strongly related to the device's impurity concentration profile and upon the material from which the device is constructed. The noise performance of the silicon double-drift structure relative to alternative structures is thus of considerable interest. A comparison is given in Figure 19(a) of the fm rms noise deviation as a function of output power for typical single and double-drift silicon and M-NN+ single-drift GaAs IMPATT diodes. In each case the diodes were mounted in the coaxial cavity illustrated in Figure 7 and the load resistance adjusted to maximize the output power with the diode biased to a junction temperature rise of 200°C. The fm noise was then measured at different values of the bias current. The results show that there is a dramatic increase in the fm noise deviation at high output powers for both the Si and GaAs single-drift devices. This behavior is in contrast to the double-drift devices which easily achieve their rated output powers with only a slight increase in Δf_{rms}.

A better indication of relative noise performance is given by the noise measure M rather than Δf_{rms} which is inversely related to the external circuit Q. M is defined by

$$M = \frac{P_o}{kT\,BW}\left[\frac{\Delta f_{rms}\,Q_{ext}'}{f_o}\right]^2 \qquad (6)$$

where BW is the measurement bandwidth[4]. The data shown in Figure 19(a) converted to noise measure vs. output power is in Figure 19(b). The GaAs IMPATT diode has the lowest noise measure at small signal but becomes considerably noisier than the double-drift IMPATT diodes at high output powers. Double-drift silicon IMPATT diodes thus have very attractive noise characteristics in addition to being capable of high efficiency and power.

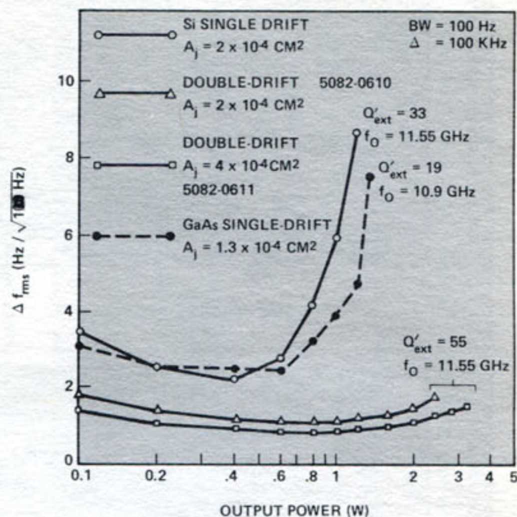

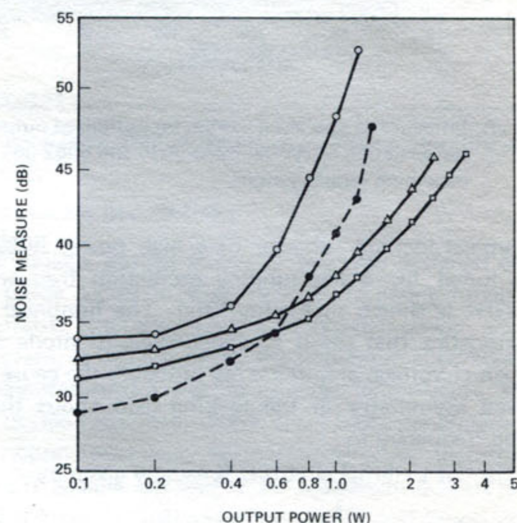

Figure 19. FM noise measured as ΔF_{rms} and computed noise measure vs. output power for 5082-0610 and 0611 double-drift Si IMPATT diodes, and for 1.2 watt Si and 1.3 watt GaAs single-drift IMPATT diodes. Efficiencies of Si and GaAs flat doping profile single-drift diodes were 7% and 11% respectively at rated output power. Q_{ext}' was determined by locking ellipse technique.

REFERENCES

1. S.M. Sze and R.R. Ryder, "Microwave Avalanche Diodes," Proc. IEEE (Special Issue on Microwave Semiconductors), 59, pp. 1140-1154, Aug. 1971.
2. D.L. Scharfetter, W.J. Evans, and R.L. Johnston, "Double-Drift Region (P+PNN+) Avalanche Diode Oscillators," Proc. IEEE (LETT.) 58, pp. 1131-1133, 1970.
3. D.L. Scharfetter and H.K. Gummel, "Large-Signal Analysis of a Silicon READ Diode Oscillator," IEEE Trans. Electron Devices, ED-16, pp. 64-77, Jan. 1969.
4. HP Application Note AN935 – Microwave Power Generation and Amplification Using IMPATT Diodes.
5. J. Monroe, "The Effect of Package Parasitics on the Stability of Microwave Negative Resistance Devices," IEEE Trans. Microwave Theory Tech., MTT-21, pp. 731-735, Nov. 1973.
6. M.S. Gupta, "Large-Signal Equivalent Circuit for IMPATT-Diode Characterization and its Application to Amplifiers," IEEE Trans. Microwave Theory Tech., MTT-21, pp. 689-694, Nov. 1973.
7. B.B. Van Iperan and H. Tjassens, "Novel and Accurate Methods for Measuring Small-Signal and Large-Signal Impedances of IMPATT Diodes," Philips Res. Repts., 27, pp. 38-75, 1972.
8. E.F. Scherer, "Large-Signal Operation of Avalanche-Diode Amplifiers," IEEE Trans. Microwave Theory Tech., MTT-18, pp. 922-932, Nov. 1970.
9. H.A. Willing, "A Two Stage IMPATT Diode Amplifier," IEEE Trans. Microwave Theory Tech., MTT-21, pp. 707-716, Nov. 1973.
10. F. Diamand and M. Armand, "External Q Factor Measurements of an Oscillator by the Injection Locking Ellipse," Electron, Lett., 8, pp. 406-407, Aug. 1972.

Hewlett Packard assumes no responsibility for the use of any circuits described herein and makes no representations or warranties, express or implied, that such circuits are free from patent infringement.

For more information, call your local HP Sales Office or East (201) 265-5000 · Midwest (312) 677-0400 · South (404) 436-6181 · West (213) 877-1282. Or, write: Hewlett-Packard, 1501 Page Mill Road, Palo Alto, California 94304. In Europe, Post Office Box 85, CH-1217, Meyrin 2, Geneva, Switzerland. In Japan, YHP, 1-59-1, Yoyogi, Shibuya-Ku, Tokyo, 151.

Printed in U.S.A. 5952-0498(2/75)